J. Fluid Mech. (2003), *vol.* 493, *pp.* 1–29.
DOI: 10.1017/S0022112003005779 Printed in the United Kingdom

On the linear stability of swept attachment-line boundary layer flow. Part 1. Spectrum and asymptotic behaviour

By DOMINIK OBRIST† AND PETER J. SCHMID

Department of Applied Mathematics, University of Washington, Seattle, WA 98195-2420, USA
pjs@amath.washington.edu

(Received 17 January 2002 and in revised form 18 April 2003)

The temporal stability of swept attachment-line boundary layer flow based on a swept Hiemenz flow model is studied. Starting from the global stability problem and motivated by analytical free-stream solutions, a Hermite expansion is employed in the chordwise coordinate direction which results in coupled local stability problems. A complete study of the temporal spectrum is presented and the discrete and continuous modes are classified according to their symmetry, chordwise polynomial order and asymptotic decay. Uniform, Görtler–Hämmerlin and higher-order modes are described in detail. Estimates are given for the location of the continuous spectrum, and bounds are derived for the validity of the linear approximation.

1. Introduction and background

Swept attachment-line boundary layer flow results when a uniform flow impinges on a blunt body whose axis forms an angle to the incoming flow. One of the most important applications is the flow near the stagnation line of swept wings.

In the 1950s experiments on swept wings with laminar airfoils detected the problem of early boundary layer transition (Gray 1952*a*, *b*). Under certain conditions the transition front of the boundary layer moved up to the attachment-line region which made it impossible to maintain laminar boundary layers over large areas of the wing. The result of this research pointed towards a critical dependence of the attachment-line region on the lift characteristics of a swept-wing airplane.

More than a decade later, experimental studies of laminar flow control demonstrated that control systems that provided suction through a perforated wing surface were not capable of laminarizing the boundary layers, once turbulent leading-edge boundary layers were established (Pfenninger 1965; Gaster 1967). Gaster (1965) pointed out that turbulent flow may be fed into the leading-edge boundary layer through the wing–fuselage junction. He suggested the use of a device (subsequently known as the Gaster bump) that decelerates the flow locally, in the wing root area, in order to relaminarize the incoming flow.

In the years following these early efforts many experimental studies have been undertaken (Gregory 1960; Gaster 1967; Cumpsty & Head 1969; Pfenninger 1977; Pfenninger & Bacon 1969) and cross-flow instabilities were suspected of being responsible for the early boundary layer transition. Poll (1979) was the first to establish

† Present address: Cray Inc., Panamaweg 7, 5034 Suhr, Switzerland.

a clear distinction between cross-flow mechanisms and instability mechanisms of the leading-edge boundary layer. His experiments on an immersed swept cylinder paved the way for theoretical developments.

Theoretical efforts on the attachment-line boundary layer go back to 1911 when Hiemenz (1911) presented in his dissertation a solution to the plane viscous stagnation-point flow which came to be known as plane Hiemenz flow – a widely accepted local model for the attachment-line flow at high Reynolds numbers. The stability of plane Hiemenz flow was first studied by Görtler (1955) and Hämmerlin (1955). They conjectured that a centrifugal instability mechanism (Görtler 1941) could render this flow unstable. However, the complex structure of this flow did not allow the use of standard techniques of linear stability theory and the reformulation into a Orr–Sommerfeld equations. In order to obtain an analytically tractable problem, they chose perturbations that exhibit the same chordwise structure as the base flow (hereafter we will refer to this model as the Görtler–Hämmerlin model). This somewhat arbitrary model was justified only much later by numerical results of Spalart (1988). In addition, Hämmerlin (1955) concluded that there exists a continuous spectrum of stationary perturbations on the real axis of the spanwise wavenumber plane.

This result was later clarified by Wilson & Gladwell (1978). They pointed out that Hiemenz flow supports two types of disturbances: disturbances that decay algebraically, and disturbances that decay exponentially in the wall-normal direction outside the boundary layer. They argued that algebraically decaying disturbances must be excluded from a physically relevant solution for several reasons (one being the exponential decay of the vorticity in the swept Hiemenz flow itself) and went on to show that the exponentially decaying modes are always stable and that they form a discrete spectrum. The continuous spectrum of Hämmerlin, so they reported, consists only of algebraically decaying modes, which they deemed irrelevant. Similar reservations about algebraically decaying modes were put forward by Kestin & Wood (1970) who noted that Hiemenz flow is an over-idealized model for the attachment-line flow.

Lyell & Huerre (1985) confirmed the linear results of Wilson & Gladwell (1978). They also presented nonlinear results using a dynamical system based on a truncated Galerkin expansion, which suggested that the flow is unstable to disturbances of large amplitude.

Further work on plane Hiemenz flow was done by Brattkus & Davis (1991). They showed how the Görtler–Hämmerlin model can be generalized for plane Hiemenz flow by expanding the perturbations in a series of chordwise Hermite polynomials. Algebraically decaying modes were further investigated by Dhanak & Stuart (1995). They showed how cross-stream vorticity in the external flow can be matched to modes that grow algebraically in the wall-normal direction. This result clearly demonstrates that modes with algebraic decay (or even growth) cannot be eliminated from a complete analysis of Hiemenz flow.

Until the work of Dallmann (1980) and Hall, Malik & Poll (1984), studies of attachment-line flow for swept wings and investigations of plane Hiemenz flow were two rather separate fields of research. Dallmann (1980) was able to recast the global stability problem of an immersed swept cylinder into a system of separable problems in which the Görtler–Hämmerlin model is but one of many chordwise modal structures. Hall *et al.* (1984) studied a flow that consisted of plane Hiemenz flow with an additional spanwise velocity component. This flow is known as swept Hiemenz flow, and is a model for the swept leading-edge boundary layer. Using the Görtler–Hämmerlin model they derived an eigenvalue problem for swept Hiemenz flow and

showed that this flow becomes unstable beyond a certain critical Reynolds number $Re_c = 583.1$. This result emphasizes the difference between two- and three-dimensional flows. Whereas plane Hiemenz flow was shown to be linearly stable, Hall *et al.* (1984) showed that introducing sweep flow can render this flow unstable. The authors were able to match their results to experimental results of Pfenninger & Bacon (1969) and Poll (1979). Following the work of Grosch & Salwen (1978) they further suggested the existence of a continuous spectrum of modes that decay algebraically in the free stream, similar to Hämmerlin's result for plane Hiemenz flow. This important work was followed by a weakly nonlinear study (see Hall & Malik 1986) where a subcritical instability was found. However, Spalart (1988), who presented the first three-dimensional direct numerical simulation (DNS) of this flow, was not able to reproduce such an instability. In a similar effort, neither Jiménez *et al.* (1990) nor Theofilis (1998), using two-dimensional DNS codes, could find Hall & Malik's solution. A subcritical instability has only been numerically observed by Joslin (1995), who presented results of a DNS with a spatial treatment of the spanwise direction.

Besides the studies based on direct numerical simulations of swept Hiemenz flow, many authors have presented further theoretical and experimental results on the swept leading-edge boundary layer. Hall & Seddougui (1990) studied perturbations other than Görtler–Hämmerlin modes in the asymptotic limit of large Reynolds numbers. Criminale, Jackson & Lasseigne (1994) studied the evolution of disturbances in inviscid stagnation-point flow, both planar and swept. Their results confirmed the findings of previous authors, i.e. that the two-dimensional flow is always stable and that the three-dimensional flow is susceptible to instabilities. This result is remarkable considering that it was obtained using inviscid theory. Theofilis (1995) addressed the spatial stability problem and Türkyilmazoğlu & Gajjar (1999) found swept Hiemenz flow to be susceptible to an absolute instability in the chordwise direction.

Lin & Malik (1996) were the first to present full modal solutions of swept Hiemenz flow that deviate from the Görtler–Hämmerlin model. They found modes with higher-order polynomial dependence in the chordwise direction. However, no method was presented to find these modes apart from solving the global stability problem directly – a prohibitively expensive task.

Bertolotti (1999) addressed the global stability problem in a different way. Similar to the idea of Brattkus & Davis (1991), he expanded the flow into a series of confluent hypergeometric functions in the chordwise direction. He was then able to confirm the polynomial modes of Lin & Malik (1996), and, in addition, find a new type of modal solution that can be connected to stationary cross-flow vortices. These new solutions relate to an earlier observation of Spalart (1988), who obtained solutions from a direct numerical simulation that were reminiscent of cross-flow vortices.

Despite a significant effort directed toward swept Hiemenz flow many features of this flow remain poorly understood, and it seems fair to state that our current knowledge of the stability characteristics of swept-leading-edge boundary layer flow lags behind our achievements in the field of parallel bounded shear flows. This is primarily due to the complex structure of swept Hiemenz flow. Most established techniques are not directly applicable and, as will be shown in this work, typical results are more involved than analogous findings for parallel shear flows. The goal of this work is then to lay the groundwork for a complete linear stability theory for swept-leading-edge boundary layer flow. Beginning with a formulation of the global stability problem for swept Hiemenz flow we will use asymptotic free-stream results to derive the appropriate chordwise dependence that will allow the separation of the global problem into (coupled) local ones. We will then discuss the nature of the full

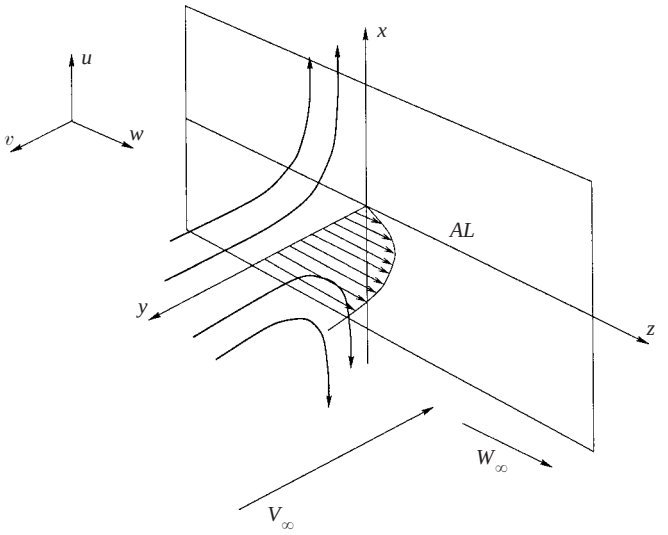

FIGURE 1. Sketch of geometry for swept attachment-line boundary layer flow.

spectrum, including discrete as well as continuous parts, and classify the modes based on their symmetry, asymptotic behaviour and chordwise dependence. All theoretical findings are confirmed by direct numerical simulations. In Part 2 (Obrist & Schmid 2003), we will discuss results of a non-modal analysis and touch upon receptivity issues based on the adjoint stability equations.

2. The global stability problem

We consider a local model for the flow near the upwind attachment-line of a swept wing. The blunt leading edge of the wing is modelled as a flat wall upon which the incoming flow impinges perpendicularly. We set the Cartesian coordinate system (x, y, z) relative to the wall, with y as the normal direction pointing upstream and x as the chordwise coordinate direction pointing away from the attachment line. The z-axis points in the spanwise direction (see figure 1).

We define a length scale $\delta^* = (\nu^*/S^*)^{1/2}$, where ν^* is the kinematic viscosity and S^* is the strain rate of the irrotational outer flow. With the free-stream sweep velocity W_∞^* the Reynolds number is defined as

$$Re = \frac{W_\infty^* \delta^*}{\nu^*}.$$

If we neglect the sweep flow, the outer flow field close to the stagnation point is described to first order by the stream function $\Psi = xy$ (Wilson & Gladwell 1978). The sweep flow can be superimposed later without changing the results. The appropriate boundary conditions for the inner solution are

$$u = v = \frac{\mathrm{d}v}{\mathrm{d}y} = w = 0 \quad \text{at} \quad y = 0,$$

$$\frac{\mathrm{d}v}{\mathrm{d}y} = -1 \qquad w = 1 \quad \text{as} \quad y \to \infty.$$

It is also consistent with the outer flow to make u linearly dependent on x, and v and w a function of y only. If we substitute this into the incompressible Navier–Stokes

equations we obtain the following system of ordinary differential equations:

$$U + V' = 0, \tag{2.1a}$$

$$V''' + (V')^2 - VV'' - 1 = 0, \tag{2.1b}$$

$$W'' - VW' = 0, \tag{2.1c}$$

with $'$ denoting differentiation with respect to y. The flow field is then given in the form

$$(u, v, w) = (Re^{-1}xU, Re^{-1}V, W). \tag{2.2}$$

This flow is known as swept Hiemenz flow. It is an exact solution to the incompressible Navier–Stokes equations. It matches the outer flow field and describes the boundary layers in the chordwise and spanwise direction. The thickness of the chordwise boundary layer given in non-dimensional units is about 2.4, whereas the spanwise boundary layer has a thickness of about 3.05. Unlike for a flat plate the boundary layer thickness does not change downstream. As (2.2) is only a valid solution in the region of the attachment line we have to bound the domain under investigation in the chordwise direction accordingly.

It is important for the later analysis to derive the asymptotic behaviour of the mean flow as the normal coordinate y tends to infinity. We obtain to leading order

$$V \sim -y, \tag{2.3a}$$

$$V' \sim -1, \tag{2.3b}$$

$$U', V'', W' \sim \mathrm{e}^{-y^2/2}. \tag{2.3c}$$

The global stability problem is derived by perturbing the laminar state, i.e. swept Hiemenz flow, by the small velocities (u', v', w'),

$$(u, v, w) = (Re^{-1}xU + u', Re^{-1}V + v', W + w').$$

These expressions are substituted into the Navier–Stokes equations which are then linearized. Separability of the spanwise (z) coordinate and time (t) calls for solutions of the form

$$\begin{pmatrix} u'(x, y, z, t) \\ v'(x, y, z, t) \\ w'(x, y, z, t) \end{pmatrix} = \begin{pmatrix} \hat{u}(x, y) \\ \hat{v}(x, y) \\ \hat{w}(x, y) \end{pmatrix} \mathrm{e}^{\mathrm{i}\beta(z-ct)}.$$

Standard algebraic and differential manipulations of the equations allow us to eliminate the pressure perturbation $\hat{p}$ as well as the spanwise velocity perturbation $\hat{w}$. The following two equations for the normal and chordwise velocity components result:

$$(\mathscr{L} + V' + \mathrm{i}\beta Re\, c)\left[\left(\partial_x^2 - \beta^2\right)\hat{u} + \partial_x\partial_y\hat{v}\right] + (\mathrm{i}\beta ReW'\partial_x - \beta^2 xV'')\hat{v} = 0, \tag{2.4a}$$

$$(\mathscr{L} - V' + \mathrm{i}\beta Re\, c)\left[\left(\partial_y^2 - \beta^2\right)\hat{v} + \partial_x\partial_y\hat{u}\right] - \left(\mathrm{i}\beta ReW'\partial_x - xV''\partial_x^2\right)\hat{u} + (\mathrm{i}\beta ReW'' + xV''\partial_x\partial_y)\hat{v} = 0, \tag{2.4b}$$

with

$$\mathscr{L} \equiv \partial_x^2 + \partial_y^2 + xV'\partial_x - V\partial_y - \beta^2 - \mathrm{i}\beta ReW. \tag{2.5}$$

Introducing the perturbation vorticities $(\hat{\psi}, \hat{\omega}, \hat{\theta})$ and using the identities

$$-\mathrm{i}\beta\hat{\psi} = \left(\partial_y^2 - \beta^2\right)\hat{v} + \partial_x\partial_y\hat{u}, \tag{2.6a}$$

$$\mathrm{i}\beta\hat{\omega} = \left(\partial_x^2 - \beta^2\right)\hat{u} + \partial_x\partial_y\hat{v}, \tag{2.6b}$$

we are able to rewrite equations (2.4) in the more compact form

$$(\mathscr{L} + V' + \mathrm{i}\beta Re\, c)\hat{\omega} - (ReW'\partial_x + \mathrm{i}\beta x V'')\hat{v} = 0, \tag{2.7a}$$

$$(\mathscr{L} - V' + \mathrm{i}\beta Re\, c)\hat{\psi} - \left(ReW'\partial_x + \frac{\mathrm{i}}{\beta}xV''\partial_x^2\right)\hat{u} + \left(ReW'' - \frac{\mathrm{i}}{\beta}xV''\partial_x\partial_y\right)\hat{v} = 0. \tag{2.7b}$$

Together with the boundary conditions

$$\hat{u} = \hat{v} = \partial_y\hat{v} = 0 \quad \text{at} \quad y = 0 \text{ and } \infty, \tag{2.8}$$

these two equations constitute the global eigenvalue problem for swept Hiemenz flow.

Close inspection shows that equation (2.4*a*) is even in x for $\hat{u}$ and odd in x for $\hat{v}$, and vice versa for (2.4*b*), which allows the introduction of a set of solutions with $\hat{u}$ even and $\hat{v}$ odd in x (which we shall call the even solutions) and a set with odd $\hat{u}$ and even $\hat{v}$ (which we shall call the odd solutions).

2.1. *Asymptotic behaviour as* $y \to \infty$

We will next seek to separate the perturbation velocities into an x-dependent and a y-dependent part. The behaviour of the global solutions as y tends to infinity will guide us in choosing the appropriate decomposition.

As the normal coordinate y tends to infinity we can make use of the asymptotic expressions for the base flow (2.3). We drop all terms in (2.7) that are (super-) exponentially small and find

$$(\bar{\mathscr{L}} + 1)\hat{\psi} = 0, \tag{2.9a}$$

$$(\bar{\mathscr{L}} - 1)\hat{\omega} = 0, \tag{2.9b}$$

with

$$\bar{\mathscr{L}} = \partial_x^2 + \partial_y^2 - x\partial_x + y\partial_y - \sigma, \tag{2.10a}$$

$$\sigma = \beta^2 + \mathrm{i}\beta Re(1 - c). \tag{2.10b}$$

In this new eigenvalue problem only the chordwise and wall-normal components of vorticity, $\hat{\psi}$ and $\hat{\omega}$, appear explicitly. The equations are only valid outside the boundary layer and are equivalent to the eigenvalue problem obtained for an inviscid swept stagnation-point flow. Solutions to this problem will be called free-stream solutions.

The operator $\bar{\mathscr{L}}$ is separable and therefore the solution of (2.9) is straightforward. We find

$$\hat{\psi}_{1,2} \sim \mathrm{He}_m(x)\mathrm{e}^{-y^2/4}\begin{cases}\mathrm{D}_{-(\sigma+m)}(y)\\ \mathrm{D}_{\sigma+m-1}(\mathrm{i}y),\end{cases} \tag{2.11a}$$

$$\hat{\omega}_{1,2} \sim \mathrm{He}_n(x)\mathrm{e}^{-y^2/4}\begin{cases}\mathrm{D}_{-(\sigma+n+2)}(y)\\ \mathrm{D}_{\sigma+n+1}(\mathrm{i}y),\end{cases} \tag{2.11b}$$

where $\mathrm{He}_n(x)$ is the Hermite polynomial of order n and $\mathrm{D}_\nu(y)$ is the parabolic cylinder function of order ν (Abramowitz & Stegun 1965). We will establish later that $n = m + 1 \equiv N$.

As $y \to \infty$ the solutions decay like

$$\hat{\psi}_{1,2} \sim \mathrm{He}_{N-1}(x) \begin{cases} y^{-(\sigma+N-1)} \mathrm{e}^{-y^2/2} \\ y^{\sigma+N-2}, \end{cases} \tag{2.12a}$$

$$\hat{\omega}_{1,2} \sim \mathrm{He}_{N}(x) \begin{cases} y^{-(\sigma+N+2)} \mathrm{e}^{-y^2/2} \\ y^{\sigma+N+1}. \end{cases} \tag{2.12b}$$

We observe two fundamentally different types of decay as y tends to infinity: either the solutions decay algebraically or they decay like $\exp(-y^2/2)$, i.e. super-exponentially. Since all modal solutions in the free stream are linear combinations of (2.11), we can classify modes into algebraically decaying and super-exponentially decaying. The trivial solution is also a valid class in which case the modal solution has vorticity in the boundary layer but not in the free stream.

3. Coupled local stability problems

We are now in a position to further manipulate the global stability problem. To this end we assume the solutions to the global stability problem to be analytic functions. Therefore it is possible to write $\hat{u}$ and $\hat{v}$ as Taylor series in x,

$$\hat{u}(x, y) = \sum_{n=0}^{\infty} x^n \hat{u}_n(y), \qquad \hat{v}(x, y) = \sum_{m=0}^{\infty} x^m \hat{v}_m(y). \tag{3.1}$$

We could substitute these expansions into (2.4), collect the coefficients of corresponding order and obtain an infinite system of ordinary differential equations in y. However, it is more promising to employ a Hermite expansion of the dependent variables. This is motivated on the one hand by the free-stream results from the previous section, and on the other hand by the suitability of this orthogonal basis for numerical purposes. Lin & Malik (1996) used a Taylor series to discretize the global stability problem in the chordwise direction which does not result in an advantageous numerical method since it is not based on an orthogonal basis. To expand the global stability problem (2.4), we therefore substitute the expansions

$$\hat{u}(x, y) = \sum_{n=0}^{\infty} \tilde{u}_n(y) \overline{\mathrm{He}}_n(x), \tag{3.2a}$$

$$\hat{v}(x, y) = \sum_{n=0}^{\infty} \tilde{v}_n(y) \overline{\mathrm{He}}_n(x). \tag{3.2b}$$

We used the normalized form $\overline{\mathrm{He}}_n(x)$ of the Hermite polynomials which are defined as

$$\overline{\mathrm{He}}_n(x) = \frac{1}{(2\pi)^{1/4}(n!)^{1/2}} \mathrm{He}_n(x), \tag{3.3}$$

and satisfy the following orthogonality relation:

$$\int_{-\infty}^{\infty} \mathrm{e}^{-x^2/2} \overline{\mathrm{He}}_m(x) \overline{\mathrm{He}}_n(x) \, \mathrm{d}x = \delta_{mn}. \tag{3.4}$$

For the chordwise operators in (2.4) we take advantage of the following relations:

$$\partial_x \overline{\mathrm{He}}_n(x) = \sqrt{n}\, \overline{\mathrm{He}}_{n-1}(x), \tag{3.5a}$$

$$x \overline{\mathrm{He}}_n(x) = \sqrt{n+1}\, \overline{\mathrm{He}}_{n+1}(x) + \sqrt{n}\, \overline{\mathrm{He}}_{n-1}(x), \tag{3.5b}$$

$$x \partial_x \overline{\mathrm{He}}_n(x) = n \overline{\mathrm{He}}_n(x) + \sqrt{n(n-1)}\, \overline{\mathrm{He}}_{n-2}(x), \tag{3.5c}$$

with similar forms for higher-order derivatives. This eliminates all operators with respect to the chordwise coordinate direction x.

In the next step we multiply the equations by $\exp(-x^2/2)\overline{\mathrm{He}}_m(x)$, integrate with respect to x and make use of the orthogonality relation of Hermite polynomials to extract equations of order m. We repeat this step for all choices of $m = 0, 1, 2, \ldots$.

Finally, exploiting the inherent chordwise symmetry of the governing equation, we regroup the dependent variables according to their symmetry in x as follows

$$\boldsymbol{q}_e = (\boldsymbol{q}_0, \boldsymbol{q}_2, \boldsymbol{q}_4, \ldots)^T, \tag{3.6}$$

$$\boldsymbol{q}_o = (\boldsymbol{q}_1, \boldsymbol{q}_3, \boldsymbol{q}_5, \ldots)^T, \tag{3.7}$$

with

$$\boldsymbol{q}_0 = (\tilde{u}_0), \quad \boldsymbol{q}_1 = (\tilde{u}_1, \tilde{v}_0)^T, \quad \boldsymbol{q}_2 = (\tilde{u}_2, \tilde{v}_1)^T, \ldots. \tag{3.8}$$

Owing to the recurrence relations (3.5) the above manipulations will yield triangular operator matrices. We obtain

$$\begin{pmatrix} \boldsymbol{P}_{0,0} & \boldsymbol{P}_{0,2} & \boldsymbol{P}_{0,4} & & & & & & & \\ & \boldsymbol{P}_{2,2} & \boldsymbol{P}_{2,4} & \boldsymbol{P}_{2,6} & & & & & & \\ & & \ddots & \ddots & \ddots & & & & & \\ & & & \ddots & \ddots & & & & & \\ & & & & \ddots & & & & & \\ & & & & & \boldsymbol{P}_{1,1} & \boldsymbol{P}_{1,3} & \boldsymbol{P}_{1,5} & & \\ & & & & & & \boldsymbol{P}_{3,3} & \boldsymbol{P}_{3,5} & \boldsymbol{P}_{3,7} & \\ & & & & & & & \ddots & \ddots & \ddots \\ & & & & & & & & \ddots & \ddots \\ & & & & & & & & & \ddots \end{pmatrix} \begin{pmatrix} \boldsymbol{q}_e \\ \boldsymbol{q}_o \end{pmatrix}$$

$$= \mathrm{i}\beta Re\, c \begin{pmatrix} \boldsymbol{Q}_{0,0} & \boldsymbol{Q}_{0,2} & & & & & & & & \\ & \boldsymbol{Q}_{2,2} & \boldsymbol{Q}_{2,4} & & & & & & & \\ & & \ddots & \ddots & & & & & & \\ & & & \ddots & & & & & & \\ & & & & & \boldsymbol{Q}_{1,1} & \boldsymbol{Q}_{1,3} & & & \\ & & & & & & \boldsymbol{Q}_{3,3} & \boldsymbol{Q}_{3,5} & & \\ & & & & & & & \ddots & \ddots & \\ & & & & & & & & \ddots & \end{pmatrix} \begin{pmatrix} \boldsymbol{q}_e \\ \boldsymbol{q}_o \end{pmatrix}, \tag{3.9}$$

where

$$\boldsymbol{P}_{m,n} = \begin{cases} S_{0,n} & \text{for } m = 0,\ n = 0 \\ (S_{0,n-1} \quad S_{0,n}) & \text{for } m = 0,\ n > 0 \\ \begin{pmatrix} R_{m-1,n-1} & R_{m-1,n} \\ S_{m,n-1} & S_{m,n} \end{pmatrix} & \text{for } m > 0,\ n > 0, \end{cases}$$

$$\mathbf{Q}_{m,n} = \begin{cases} a_{0,0}\beta^2 & \text{for } m = n = 0 \\ (-a_{0,1}\partial_y \quad 0) & \text{for } m = 0,\ n = 2 \\ \begin{pmatrix} a_{m-1,0}\left(\beta^2 - \partial_y^2\right) & -a_{m-1,1}\partial_y \\ 0 & a_{m,0}\beta^2 \end{pmatrix} & \text{for } m = n > 0 \\ \begin{pmatrix} 0 & 0 \\ -a_{m,1}\partial_y & -a_{m,2} \end{pmatrix} & \text{for } m = (n-2) > 0, \end{cases}$$

with

$$\begin{aligned} R_{m-1,m-1} &= a_{m-1,0}\left[(\mathscr{L}_y + (m-2)V')\left(\partial_y^2 - \beta^2\right) + (m-1)V''\partial_y + \mathrm{i}\beta ReW''\right], \\ R_{m-1,m} &= a_{m-1,1}[(\mathscr{L}_y + (m-2)V')\partial_y + (m-1)V'' - \mathrm{i}\beta ReW'], \\ R_{m-1,m+1} &= a_{m-1,2}\left[(1+V')\left(\partial_y^2 - \beta^2\right) + V''\partial_y\right], \\ R_{m-1,m+2} &= a_{m-1,3}[(1+V')\partial_y + V''], \\ S_{m,m-1} &= a_{m-1,1}[-\beta^2 V''], \\ S_{m,m} &= a_{m,0}[-\beta^2(\mathscr{L}_y + (m+1)V')], \\ S_{m,m+1} &= a_{m,1}[(\mathscr{L}_y + (m+1)V')\partial_y + \mathrm{i}\beta ReW' - \beta^2 V''], \\ S_{m,m+2} &= a_{m,2}[(\mathscr{L}_y + (m+1)V') - \beta^2(1+V')], \\ S_{m,m+3} &= a_{m,3}[(1+V')\partial_y], \\ S_{m,m+4} &= a_{m,4}[1+V'], \end{aligned}$$

and

$$\mathscr{L}_y = \partial_y^2 - V\partial_y - \beta^2 - \mathrm{i}\beta ReW,$$

$$a_{m,n} = \sqrt{\frac{(m+n)!}{m!}}.$$

The matrices in (3.9) are triangular and the set of eigenvalues for (3.9) is equivalent to the union of the eigenvalues of the diagonal terms. It is therefore sufficient to solve for the eigenvalues of each diagonal block separately. Each one of these separated eigenvalue problems yields a set of eigenfunctions $\{\boldsymbol{q}_m\} = \{(\tilde{u}_m, \tilde{v}_{m-1})\}$. Substituting these eigensolutions back into the global system (3.9) results in forced solutions for all $\boldsymbol{q}_{m-2j}$ and trivial solutions for all other $\boldsymbol{q}_n$. Thus, there is a finite number of non-zero Hermite coefficients, which is equivalent to the important fact that all modes are polynomials in x. One exception to this finding will be presented in the conclusions.

In the following sections we present numerical solutions of (3.9). The wall-normal operators are discretized using a Chebyshev spectral collocation method with a rational map of the semi-infinite domain onto the interval $[-1, 1]$ (see Boyd 1982, 1987).

4. Numerical results

To find the eigenvalues c of the global stability problem it suffices to obtain the eigenvalues of the block diagonal systems of (3.9).

The eigenvalue problem of order N is

$$\left[\partial_y^2 - V\partial_y - \beta^2 + (N+1)V' - \mathrm{i}\beta ReW\right]\hat{u}_N + V''\hat{v}_{N-1} = -\mathrm{i}\beta Re\, c\,\hat{u}_N, \qquad (4.1a)$$

$$\begin{aligned} &\left[\left(\partial_y^2 - V\partial_y - \beta^2 + (N-2)V' - \mathrm{i}\beta ReW\right)\left(\partial_y^2 - \beta^2\right) - V''\partial_y - NV''' + \mathrm{i}\beta ReW''\right]\hat{v}_{N-1} \\ &\quad - 2N(V'' + V'\partial_y)\hat{u}_N = -\mathrm{i}\beta Re\, c\left(\partial_y^2 - \beta^2\right)\hat{v}_{N-1}, \end{aligned} \qquad (4.1b)$$

with the boundary conditions

$$\hat{u}_N = \hat{v}_{N-1} = \partial_y \hat{v}_{N-1} = 0 \quad \text{at} \quad y = 0 \text{ and } \infty.$$

This system of equations is equivalent to the block diagonal subsystems of (3.9).

4.1. *Asymptotic behaviour as* $y \to \infty$

To arrive at asymptotic results we let y tend to infinity and omit the exponentially small terms in (4.1) as we did in § 2.1 for the global problem. We obtain

$$\left[\partial_y^2 + y\partial_y - \beta^2 - (N+1) - \mathrm{i}\beta Re(1-c)\right]\hat{u}_N = 0, \tag{4.2a}$$

$$\left[\partial_y^2 + y\partial_y - \beta^2 - (N-2) - \mathrm{i}\beta Re(1-c)\right]\left(\partial_y^2 - \beta^2\right)\hat{v}_{N-1} = -2N\partial_y \hat{u}_N. \tag{4.2b}$$

These equations can be transformed into parabolic cylinder equations. Moreover, (4.2*a*) is homogeneous. The solution of this equation yields an inhomogeneity for (4.2*b*). We obtain an intermediate result that can be expressed in terms of parabolic cylinder functions $\mathrm{D}_\nu(y)$ as follows:

$$\begin{pmatrix} \hat{u}_N \\ \left(\partial_y^2 - \beta^2\right)\hat{v}_{N-1} \end{pmatrix}_a \sim \mathrm{e}^{-y^2/4} \begin{pmatrix} \mathrm{D}_{-\nu-1}(\mathrm{i}y) \\ -\mathrm{i}N(1+\nu)\mathrm{D}_{-\nu-2}(\mathrm{i}y) \end{pmatrix}, \tag{4.3a}$$

$$\begin{pmatrix} \hat{u}_N \\ \left(\partial_y^2 - \beta^2\right)\hat{v}_{N-1} \end{pmatrix}_b \sim \mathrm{e}^{-y^2/4} \begin{pmatrix} \mathrm{D}_{\nu}(y) \\ -N\mathrm{D}_{\nu+1}(y) \end{pmatrix}, \tag{4.3b}$$

$$\begin{pmatrix} \hat{u}_N \\ \left(\partial_y^2 - \beta^2\right)\hat{v}_{N-1} \end{pmatrix}_c \sim \mathrm{e}^{-y^2/4} \begin{pmatrix} 0 \\ \mathrm{D}_{-\nu-4}(\mathrm{i}y) \end{pmatrix}, \tag{4.3c}$$

$$\begin{pmatrix} \hat{u}_N \\ \left(\partial_y^2 - \beta^2\right)\hat{v}_{N-1} \end{pmatrix}_d \sim \mathrm{e}^{-y^2/4} \begin{pmatrix} 0 \\ \mathrm{D}_{\nu+3}(y) \end{pmatrix}, \tag{4.3d}$$

with

$$\nu = -[N + 2 + \beta^2 + \mathrm{i}\beta Re(1-c)].$$

As a final step we have to invert the operator $(\partial_y^2 - \beta^2)$. Although this task is straightforward and the solution can be expressed in terms of integrals, it is more useful to give the leading-order behaviour of the solutions as $y \to \infty$. There are now six fundamental solutions due to the two additional homogeneous solutions of $(\partial_y^2 - \beta^2)\hat{v}_{N-1} = 0$. We find

$$\begin{pmatrix} \hat{u}_N \\ \hat{v}_{N-1} \end{pmatrix}_a \sim \begin{pmatrix} y^{-\nu-1} \\ \mathrm{i}N\beta^{-2}(1+\nu)y^{-\nu-2} \end{pmatrix}, \quad \begin{pmatrix} \hat{u}_N \\ \hat{v}_{N-1} \end{pmatrix}_b \sim \begin{pmatrix} y^{\nu}\mathrm{e}^{-y^2/2} \\ -Ny^{\nu-1}\mathrm{e}^{-y^2/2} \end{pmatrix}, \tag{4.4a, b}$$

$$\begin{pmatrix} \hat{u}_N \\ \hat{v}_{N-1} \end{pmatrix}_c \sim \begin{pmatrix} 0 \\ y^{-\nu-4} \end{pmatrix}, \quad \begin{pmatrix} \hat{u}_N \\ \hat{v}_{N-1} \end{pmatrix}_d \sim \begin{pmatrix} 0 \\ y^{\nu+1}\mathrm{e}^{-y^2/2} \end{pmatrix}, \tag{4.4c, d}$$

$$\begin{pmatrix} \hat{u}_N \\ \hat{v}_{N-1} \end{pmatrix}_e \sim \begin{pmatrix} 0 \\ \mathrm{e}^{\beta y} \end{pmatrix}, \quad \begin{pmatrix} \hat{u}_N \\ \hat{v}_{N-1} \end{pmatrix}_f \sim \begin{pmatrix} 0 \\ \mathrm{e}^{-\beta y} \end{pmatrix}. \tag{4.4e, f}$$

Up to differences in the solutions for $\hat{v}_{N-1}$ this is the generalized form of the asymptotic solutions that were given by Hall *et al.* (1984).

The solutions (4.4*a*, *b*) are homogeneous solutions of (4.2*a*) and particular solutions of (4.2*b*), and (4.4*c*–*f*) are homogeneous solutions of (4.2*b*). The two exponential solutions (4.4*e*, *f*) correspond to the case where the chordwise vorticity $\hat{\psi}$ vanishes outside the boundary layer.

In (4.4*a–d*) we recognize the algebraic and super-exponential decay in y of the free-stream solutions (2.12). The trivial case of the free-stream solutions corresponds to (4.4*e*, *f*).

The solution (4.4*e*) has to be discarded since it grows without bounds as $y \to \infty$; (4.4*b*, *d*, *f*) will always satisfy the homogeneous boundary condition. The algebraically decaying solutions (4.4*a*, *c*) are only valid for negative exponents. This yields a constraint on the eigenvalues $c = c_r + \mathrm{i}c_i$ for the algebraically decaying modes,

$$c_i < -\frac{N+1+\beta^2}{\beta Re} \quad \text{for } (\hat{u}_N, \hat{v}_{N-1})_a \tag{4.5a}$$

$$c_i < -\frac{N-2+\beta^2}{\beta Re} \quad \text{for } (\hat{u}_N, \hat{v}_{N-1})_c, \tag{4.5b}$$

from which we conclude that unstable algebraically decaying modes of type (4.4*c*) are possible for $N = 1$ but for no other choice of N. There is no constraint on c_r. For $c_r = 1$ the exponents are real and we obtain waves travelling with the free-stream sweep flow decaying algebraically far away from the wall. For $c_r \neq 1$ the exponents have imaginary parts and the solutions oscillate in y as $\exp[\mathrm{i}\beta Re(1-c_r)\ln y]$ with a decaying amplitude.

By studying the asymptotic behaviour of the eigenvalue problem (4.1) we have found five different fundamental solutions. We can classify these solutions into algebraically, exponentially, and super-exponentially decaying solutions. We will now proceed to study numerical solutions of the separated eigenvalue problems for different orders N. The asymptotic results will help us to understand and classify the numerical solutions.

4.2. *Uniform modes*

The simplest case is $N = 0$. The wall-normal velocity component $\hat{v}$ is zero and the chordwise velocity $\hat{u}_0$ is a function of y only. From the continuity equation we know that the spanwise velocity component $\hat{w}$ is zero as well. Therefore these modes represent uniform disturbance fields in the chordwise direction with varying amplitude in the wall-normal and spanwise directions. The eigenvalue problem (4.2) reduces to a much simpler problem with only one dependent variable,

$$\left[\partial_y^2 - V\partial_y + V' - \beta^2 - \mathrm{i}\beta ReW\right]\hat{u}_0 = -\mathrm{i}\beta Re\, c\, \hat{u}_0, \tag{4.6a}$$

$$\hat{u}_0(0) = \hat{u}_0(\infty) = 0. \tag{4.6b}$$

We transform the dependent variable according to

$$\hat{u}_0(y) = \exp\left[\frac{1}{2}\int^y V\,\mathrm{d}y\right]\bar{u}(y) \sim \mathrm{e}^{-y^2/4}\,\bar{u}(y)$$

to obtain the modified eigenvalue problem

$$\bar{u}'' + \left[\tfrac{3}{2}V' - \tfrac{1}{4}V^2 - \beta^2 - \mathrm{i}\beta Re(W-c)\right]\bar{u} = 0. \tag{4.7}$$

As before we find that this equation approaches a parabolic cylinder equation in the limit as $y \to \infty$. One of the two solutions behaves like

$$\bar{u} \sim \mathrm{D}_{-\nu-1}(\mathrm{i}y)$$

with $\nu = -[2+\beta^2+\mathrm{i}\beta Re(1-c)]$. As we transform this solution back to $\hat{u}_0$ we obtain algebraically decaying solutions of type (4.4*a*). The constraint (4.5*a*) on the eigenvalue

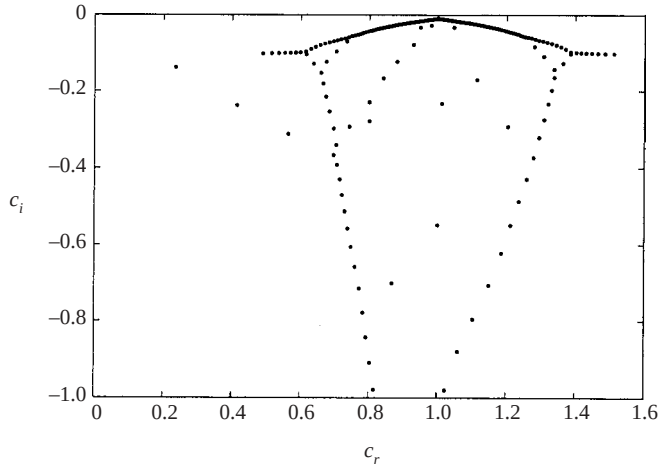

FIGURE 2. Spectrum of the uniform modes for $\beta = 0.3$ and $Re = 1000$.

c shows us that these modes are stable,

$$c_i < -\frac{1+\beta^2}{\beta Re} < 0.$$

The second solution of the parabolic cylinder equation,

$$\bar{u} \sim \mathrm{D}_v(y),$$

represents modes which decay super-exponentially like (4.4b).

Figure 2 shows the spectrum of the uniform modes solved on a grid with $N_y = 500$ collocation points that is stretched toward infinity with half of the collocation points clustered in the interval $[0, y_{\mathrm{half}}]$. We choose $y_{\mathrm{half}} = 10$. The numerically computed eigenvalues form a line across the complex c-plane with a cusp close to $c = 1$. Inspection of the eigenfunctions corresponding to the eigenvalues on that line shows that these are all algebraically decaying solutions of (4.6). The eigenvalues below this line are mostly algebraically decaying modes as well and we have to assume that the spectrum of algebraically decaying modes is continuous and covers large areas of the half-plane below the maximal c_i.

If we solve the eigenvalue problem (4.7) instead of (4.6) but still use homogeneous boundary conditions $\bar{u}(0) = \bar{u}(\infty) = 0$, we obtain only eigensolutions of type (4.4b) since the algebraically decaying modes are excluded due to the boundary condition at infinity. A numerical result (number of collocation points $N_y = 500$, extent of the computational domain $y_{\max} = 1000$ with half the collocation points in $0 \leqslant y \leqslant y_{\mathrm{half}} = 10$) is shown in figure 3.

We find that besides seven discrete modes $c_0, \ldots, c_6$ there is a continuous line spectrum along $c_r = 1, c_i < 0$ which is represented numerically by the vertical line originating near $c_r = 1, c_i \approx 0$. The eigenfunctions of the seven discrete modes are shown in figure 4. The maximum amplitude moves farther away from the wall with increasing real part of the eigenvalue. This is consistent with the concept of the critical layer y_c determined by $W(y_c) = c_r$ (see Drazin & Reid 1981).

We can study the decay in the wall-normal direction of the discrete modes by plotting the solutions $\bar{u}(y)$ on a logarithmic scale (figure 5). From the asymptotic solution (4.4b) we expect super-exponential decay. However, it appears that the eigenfunctions

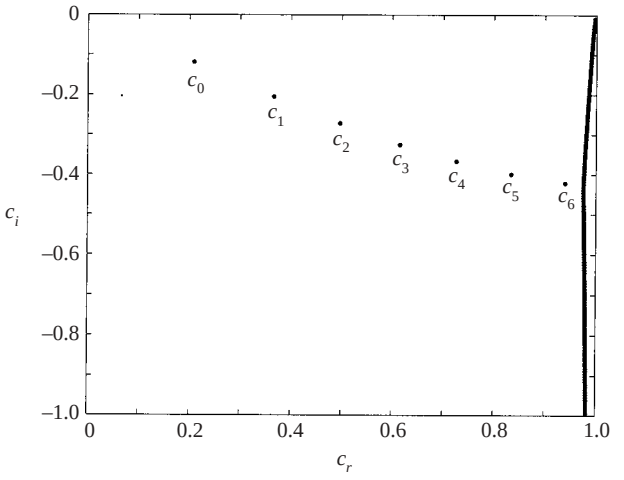

FIGURE 3. Spectrum of the exponentially decaying uniform modes for $\beta = 0.3$ and $Re = 1000$.

decay exponentially outside the boundary layer. Except for the slowest decaying mode c_6, the onset of the super-exponential decay is below numerical accuracy and therefore cannot be seen in figure 5. Obviously, there is an interval where exponential decay is observed, before the super-exponential decay begins. We interpret this interval as an internal layer between the boundary layer solution and the parabolic cylinder function of the outer layer.

In order to explain this internal layer we take a closer look at (4.7). For $\beta Re|1-c| \gg 1$, the term $\mathrm{i}\beta Re(W-c)$ dominates the other terms in the square bracket of (4.7) for $1 \ll y \ll 2(\beta Re|1-c|)^{1/2}$. The internal layer solution $\bar{u}_i$ is therefore governed by the equation

$$\bar{u}_i'' - \mathrm{i}\beta Re(1-c)\bar{u}_i = 0, \tag{4.8}$$

where we have replaced W by 1, since the internal layer is outside the boundary layer. There are two fundamental solutions. The decaying solution for the internal layer is given by

$$\bar{u}_i = \exp\bigl(-[\mathrm{i}\beta Re(1-c)]^{1/2} y\bigr). \tag{4.9}$$

The internal-layer solution is shown in figures 5 and 6 for the slowest decaying mode c_6. Clearly, the internal-layer solution (4.9) is a good approximation to the eigenfunction. It is also noteworthy that the upper limit of the internal layer interval (at $y \approx 22.61$; not shown in figure 5) provides a good estimate for the onset of the super-exponential decay. Three additional results can be stated from our analysis of the internal layer.

(*a*) There is a square-root branch cut in the complex c-plane originating from the exponent of the internal-layer solution (4.9). The branch point is at $c = 1$. This branch cut is associated with the continuous line spectrum (see also Gustavsson 1979).

(*b*) On the branch cut along $c_r = 1$, $c_i < 0$ neither solution of (4.8) decays.

(*c*) For the algebraically decaying modes there is no internal layer, thus there is no branch cut and eigenvalues with $c_r > 1$ exist. Eigenvalues with $c_r > 1$ relate to the concept of leaky waves (P. Luchini, private communication; Marcuse 1991).

We complete our discussion of the uniform modes by comparing the solutions for different values of β and Re. We find that the solutions are to first order a function of βRe since for $Re \gg \beta$ – which is the case for the studied parameter range – the

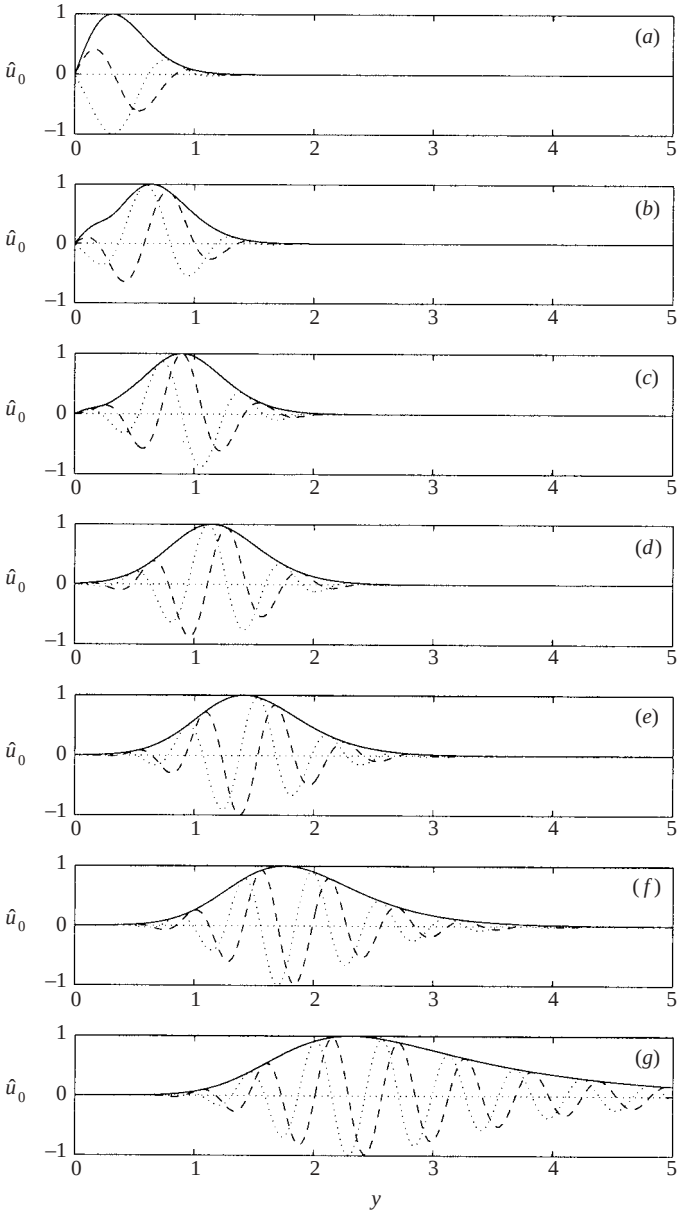

FIGURE 4. Absolute value (——), and real (– – –), and imaginary (· · ·) parts of the eigenfunctions of the discrete uniform modes (*a*) c_0, (*b*) $c_1, \ldots,$ (*g*) c_6 for $\beta = 0.3$ and $Re = 1000$.

contribution of β^2 in (4.7) is negligible. Figure 7 shows a scatter plot of the location of the first four discrete eigenvalues for different values of βRe. The location of the eigenvalues approximately obeys the power law

$$c \propto (\beta Re)^{-1/3}. \tag{4.10}$$

4.3. *Görtler–Hämmerlin modes*

For $N = 1$ we obtain the classical Görtler–Hämmerlin eigenvalue problem first discussed by Hämmerlin (1955) and Görtler (1955) for the (unswept) plane case, and

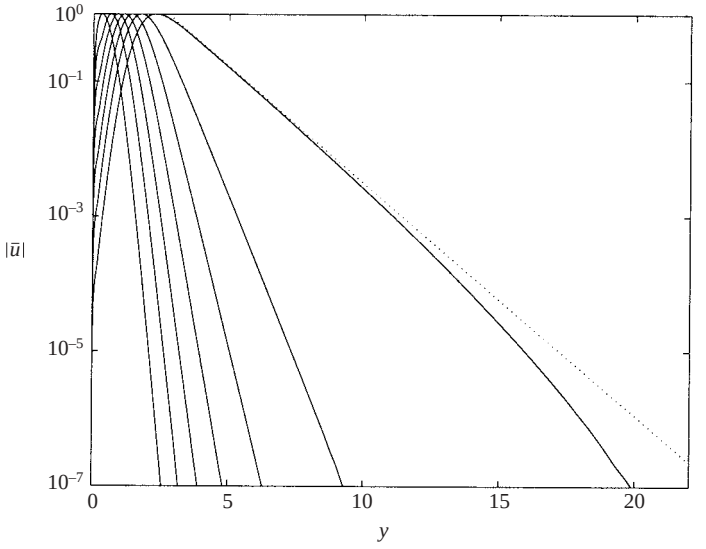

FIGURE 5. Absolute value $|\bar{u}|$ (——) of the seven discrete modes for $\beta = 0.3$ and $Re = 1000$, and the internal-layer solution for the slowest decaying eigenfunction (· · ·).

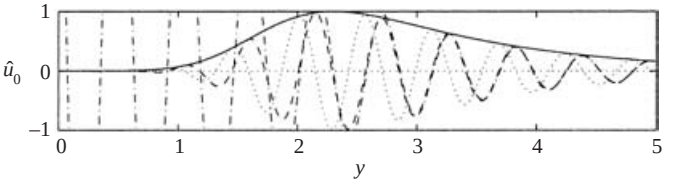

FIGURE 6. Absolute value (——), and real (– – –), and imaginary (· · ·) parts of the most stable discrete uniform mode c_6 for $\beta = 0.3$ and $Re = 1000$, and the real part of the internal-layer solution (– · –).

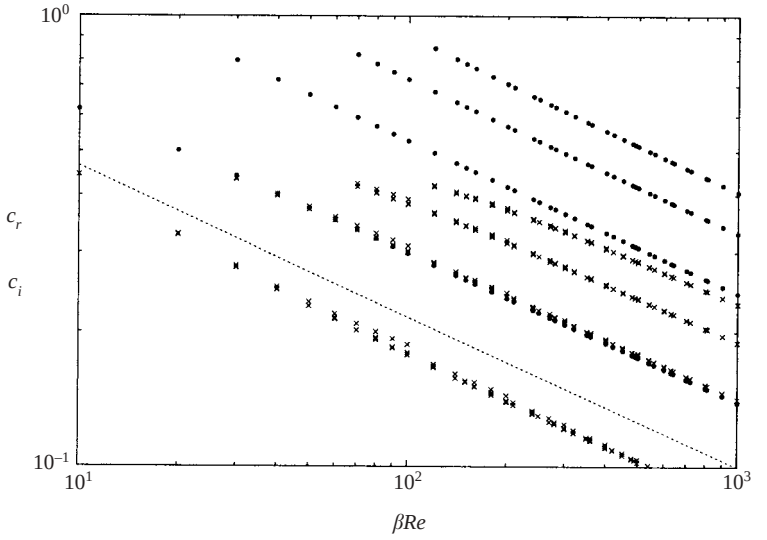

FIGURE 7. Scatter plot of the real (•) and negative imaginary parts (×) of the first four discrete modes for different values of βRe, compared to $(\beta Re)^{-1/3}$ (– – –).

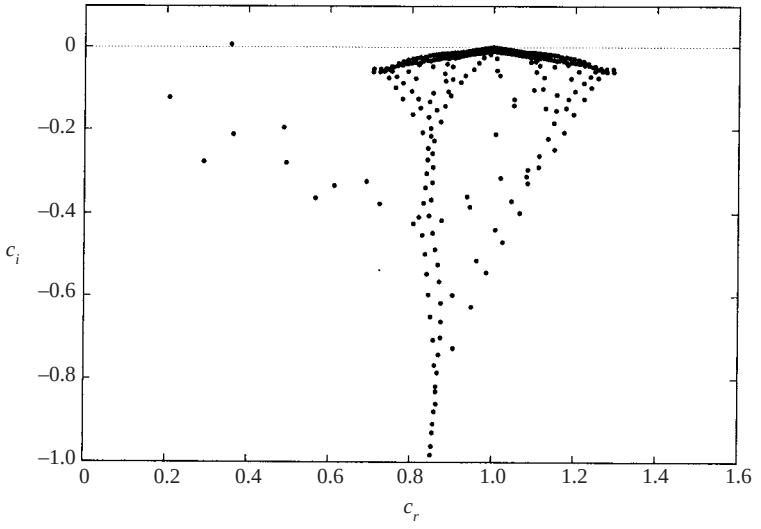

FIGURE 8. Spectrum of the Görtler–Hämmerlin modes for $\beta = 0.3$ and $Re = 1000$.

later by Hall *et al.* (1984) for the (swept) three-dimensional case. A numerical solution for the eigenvalues for $\beta = 0.3$ and $Re = 1000$ is shown in figure 8. It was computed on a grid with 250 points stretched toward infinity with $y_{\text{half}} = 10$. We observe similar phenomena to those in the uniform case ($N = 0$). There are two distinct spectra of algebraically decaying modes forming lines across the complex c-plane with cusps at $c_r = 1$. One spectrum corresponds to modes that decay like (4.4a), i.e. both velocity components decay algebraically. The other spectrum corresponds to solutions of type (4.4c) where only $\hat{v}_0$ decays algebraically and $\hat{u}_1$ vanishes super-exponentially outside the boundary layer. The latter contains unstable modes. The Görtler–Hämmerlin problem is the only choice for N that supports unstable algebraically decaying modes. Figure 9 shows eigenfunctions of the two algebraic spectra together with their asymptotic solutions (4.4a, c). For the modes of type (4.4c) the wall-normal velocity component is dominant. For the modes of type (4.4a) the amplitude of $\hat{u}_1$ eventually exceeds the amplitude of $\hat{v}_0$ due to its slower decay rate.

Since the algebraic modes cover large areas of the complex c-plane it is difficult to extract and study other modes. We therefore transform the dependent variables according to

$$\begin{pmatrix} \hat{u}_1 \\ \hat{v}_0 \end{pmatrix} = \mathrm{e}^{-\alpha y} \begin{pmatrix} \bar{u}_1 \\ \bar{v}_0 \end{pmatrix}, \tag{4.11}$$

where we choose $0 < \alpha < \beta$. Under this transformation algebraically decaying modes will not satisfy the homogeneous boundary conditions at infinity and we obtain a spectrum as shown in figure 10 ($N_y = 100$, $y_{\text{half}} = 1$, $\alpha = 0.1$).

There are three distinct branches of discrete modes. The upper branch contains the unstable mode, i.e. the Tollmien–Schlichting mode, with a phase velocity of 0.3574 and a growth rate of 0.006126. All eigenfunctions of this branch show a strong dominance of the wall-normal velocity component over the chordwise velocity. The amplitude of the chordwise velocity reaches approximately 1% of the maximum amplitude of the wall-normal velocity component (figure 11a). The next lower branch contains eigenvalues that are at nearly the same locations as the discrete uniform modes. The $\hat{u}_1$ component of the corresponding eigenfunctions matches the uniform

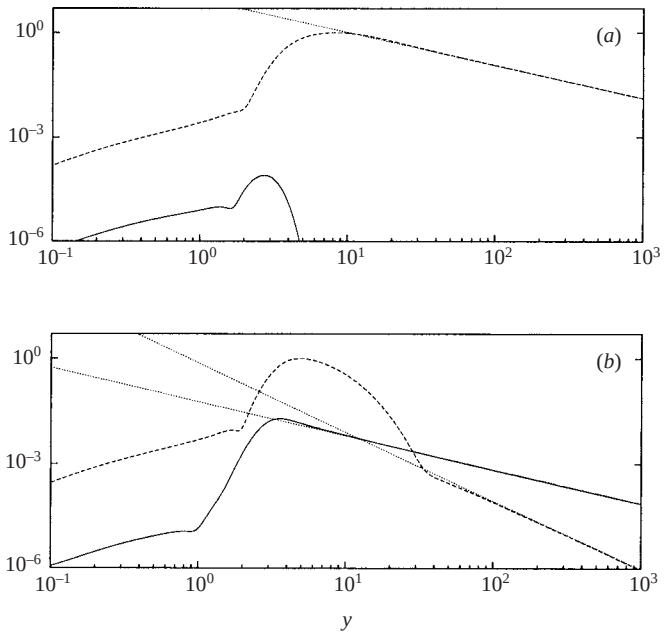

FIGURE 9. Absolute values of eigenfunctions for (*a*) $c = 1.00854 - \mathrm{i}\,0.0018181$ (type 4.4*c*), and (*b*) $c = 0.998098 - \mathrm{i}\,0.0101945$ (type 4.4*a*) for $\beta = 0.3$ and $Re = 1000$: ——, $|\hat{u}_1|$; – – –, $|\hat{v}_0|$; · · ·, asymptotic solutions.

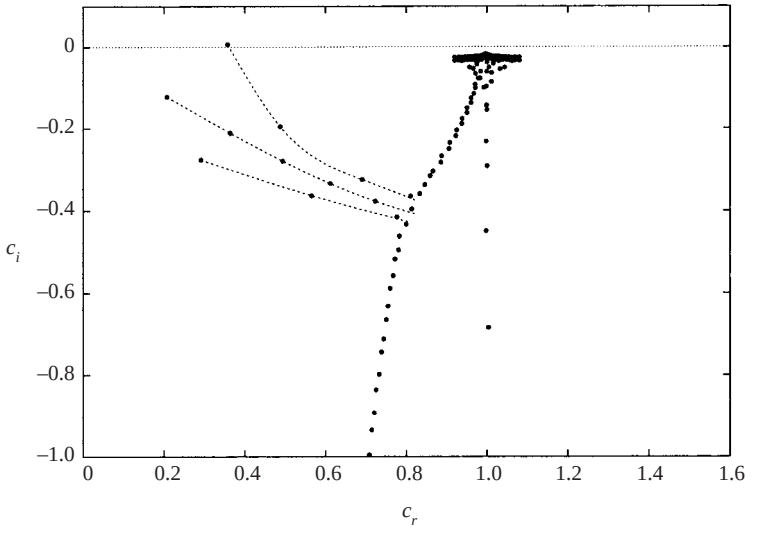

FIGURE 10. Spectrum of the exponentially decaying Görtler–Hämmerlin modes for $\beta = 0.3$ and $Re = 1000$; the upper, lower, and uniform branches are highlighted by dashed lines.

eigenfunctions closely, whereas $\hat{v}_0$ is small compared to $\hat{u}_1$ inside the boundary layer and dominates only in the free stream (figure 11*b*). We will refer to this branch as the uniform branch. Finally, there is the lower branch which contains modes similar to the upper branch in the sense that the chordwise velocity is small compared to the wall-normal velocity (figure 11*c*).

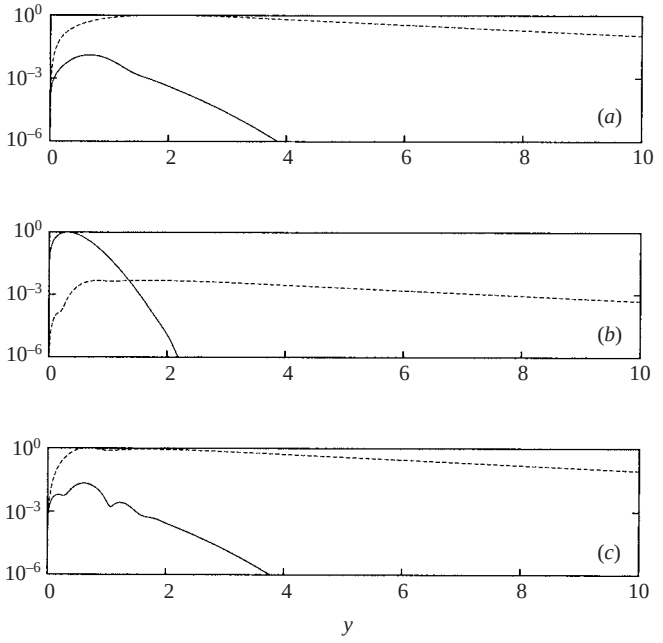

FIGURE 11. Absolute values of Görtler–Hämmerlin eigenfunctions for (*a*) $c = 0.3574 + \mathrm{i}\,0.006126$ (Tollmien–Schlichting mode), (*b*) $c = 0.2071 - \mathrm{i}\,0.1223$ (least-stable mode of the uniform branch), and (*c*) $c = 0.2917 - \mathrm{i}\,0.2765$ (least stable mode of lower branch) for $\beta = 0.3$ and $Re = 1000$: ——, $|\hat{u}_1|$; – – –, $|\hat{v}_0|$.

We observe two branches of a continuous spectrum. Their exact location could not be determined numerically nor analytically. However, from what we have learned about the continuous line spectrum in the uniform case ($N = 0$), it is reasonable to assume their correct location to be $c_r = 1$, $c_i < 0$. The eigenfunctions of these continuous line spectra show a dominance of either the chordwise or wall-normal velocity. Therefore, we relate the continuous line spectra to either the uniform branch or the upper and lower branches corresponding to the dominant velocity.

All modes in the spectrum shown in figure 10 decay exponentially in $\hat{v}_0$ and super-exponentially in $\hat{u}_1$, i.e. like a linear combination of (4.4*a*) and (4.4*f*). No modes could be found that decay super-exponentially for both $\hat{u}_1$ and $\hat{v}_0$. At least one component must decay either algebraically or exponentially.

We again conclude this section by studying the influence of the parameters β and Re on the location of the eigenvalues. We find that the eigenvalues of the uniform and the lower branches are proportional to $(\beta Re)^{-1/3}$ which is identical to the result (4.10) found for the uniform case ($N = 0$). The eigenvalues of the upper branch do not follow this simple law. The complex dependence of the eigenvalues of the upper branch on the parameters β and Re is demonstrated in figure 12. It shows the paths the Tollmien–Schlichting mode takes as β changes its value continuously for different values of Re. We detect a range of parameters β and Re for which the Tollmien–Schlichting mode is unstable. The neutral stability curve shown in figure 13 defines this parameter range. Such a curve was first presented by Hall *et al.* (1984).

4.4. *Higher-order modes*

The spectra for higher values of N show the same qualitative structure as the Görtler–Hämmerlin spectrum. There are two continuous spectra of algebraically decaying

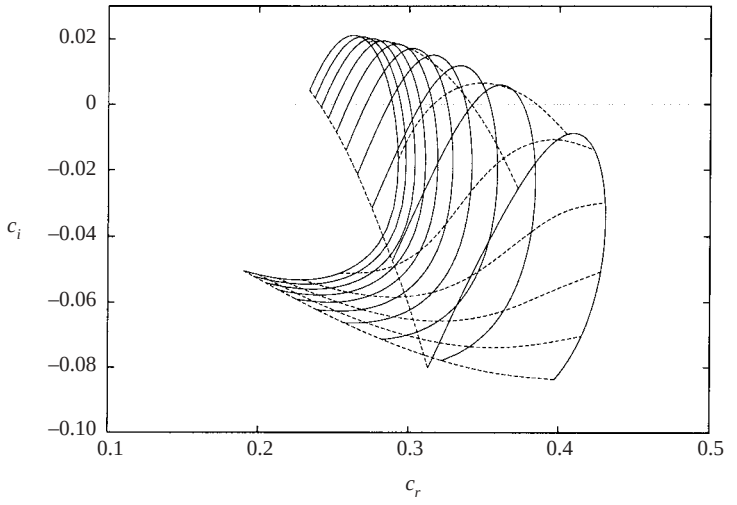

FIGURE 12. Path of the locus of the Tollmien–Schlichting mode for β ranging from 0.1 to 0.8 and Re held constant at the values $Re = 400, 800, \ldots, 4000$; lines for constant β are dashed; the rightmost curve is for $Re = 400$; as β increases the eigenvalue moves along the curves in a clockwise direction.

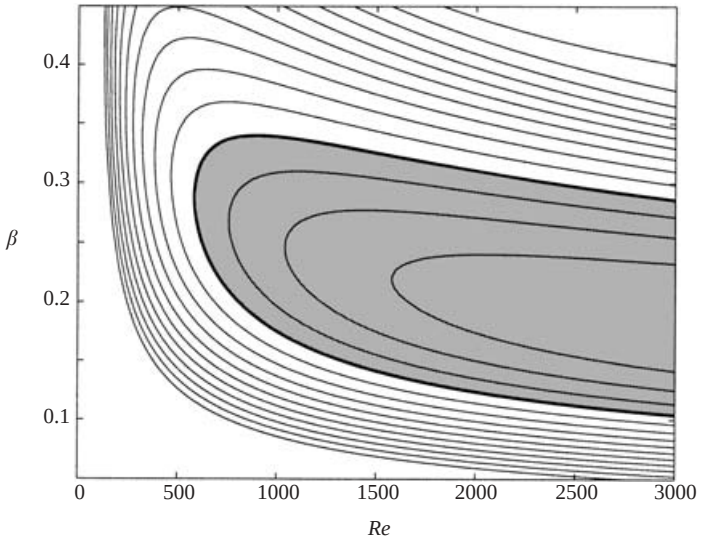

FIGURE 13. Neutral stability curve for the swept Hiemenz flow. The contour values of the growth rate range from -0.05 to $+0.02$ with a contour spacing of 0.005. The shaded area represents parameter values that result in an exponential instability.

modes, two continuous line spectra, and the three branches of discrete modes in approximately the same position relative to each other. A significant difference with the Görtler–Hämmerlin spectrum is that the whole spectrum is shifted to lower imaginary values, i.e. higher-order modes are more damped. This is obvious for the algebraically decaying modes for which we showed that their spectrum is bounded by (4.5). This bound decreases linearly with increasing N. For the exponentially decaying modes there is no such bound and we have to rely on numerical evidence in the form

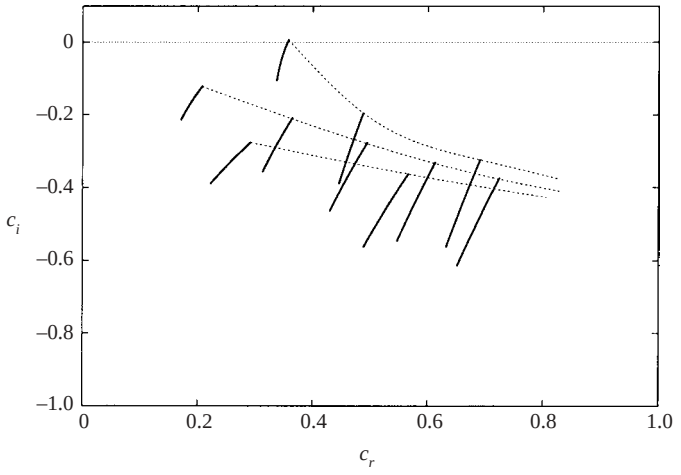

FIGURE 14. The ten least stable discrete eigenvalues for $N = 0, 1, \ldots, 100$, $\beta = 0.3$, $Re = 1000$; the upper, lower, and uniform branches for $N = 1$ are highlighted by dashed lines.

of figure 14, where discrete eigenvalues for $N = 0, 1, \ldots, 100$ are shown. The figure suggests that as N is increased the discrete modes move to lower imaginary values.

Figures 15 and 16 show several eigenfunctions and their lower-order forced solutions for $N = 4$ and $N = 5$. The eigenfunctions $\{\boldsymbol{q}_N\} = \{\hat{u}_N, \hat{v}_{N-1}\}$ show the same characteristics as the Görtler–Hämmerlin eigenfunctions: the decay of the algebraic eigenfunctions follows (4.4*a*, *c*). The discrete modes and the modes of the continuous line spectra decay super-exponentially in $\hat{u}_N$ and exponentially in $\hat{v}_{N-1}$ like (4.4*f*). The chordwise velocity component is predominant inside the boundary layer for the modes of the uniform branch and vice versa for the modes of the upper and lower branches. Note the similar shape of the corresponding eigenfunctions $(\hat{u}_1, \hat{v}_0)$ in figures 11(*a*, *b*), $(\hat{u}_4, \hat{v}_3)$ in figures 15(*a*, *b*), and $(\hat{u}_5, \hat{v}_4)$ in figures 16(*a*, *b*).

The decay of the forced lower-order solutions does not follow the asymptotic expressions (4.4). The decay of both lower-order velocity components of the discrete modes is governed by $\exp(-\beta y)$ and they have larger amplitudes than the eigenfunctions. As we proceed from the eigenfunctions $\{\boldsymbol{q}_N\}$ to lower orders, $\{\boldsymbol{q}_N\} \mapsto \{\boldsymbol{q}_{N-2}\} \mapsto \{\boldsymbol{q}_{N-4}\} \mapsto \ldots$, the solutions are increasingly amplified. The lowest-order solutions – either $\{\boldsymbol{q}_0\}$ for N even or $\{\boldsymbol{q}_1\}$ for N odd – are the most amplified.

We obtain similar results for the algebraically decaying modes (figures 15*c*, *d* and 16*c*, *d*). The lower-order solutions are again amplified and both velocity components decay algebraically. The lower-order solutions of modes of type (4.4*a*) maintain the decay rate of the corresponding eigenfunction, whereas the lower-order solutions of type (4.4*c*) decay like $y^{-\nu-5}$ and $y^{-\nu-6}$, respectively.

As we reassemble the modal solutions into a flow field $(\hat{u}(x, y), \hat{v}(x, y))$ we observe a distinct pattern of the predominant direction of the flow field for discrete modes of even and odd orders N. We distinguish between four different regions in the flow field:

(*a*) Close to the attachment line ($x = O(1)$, $y = O(1)$) the direction of the flow is governed by the lowest-order solution $\boldsymbol{q}_0$ or $\boldsymbol{q}_1$, respectively. In even modes the chordwise velocity therefore dominates; for odd N the predominant direction of the flow is chordwise for modes of the uniform branch and wall-normal for modes from the upper and lower branches.

(*b*) As we move away from the wall while keeping x moderate ($x = O(1)$, $y \gg 1$) the asymptotic decay of the lowest-order solution determines the predominant direction

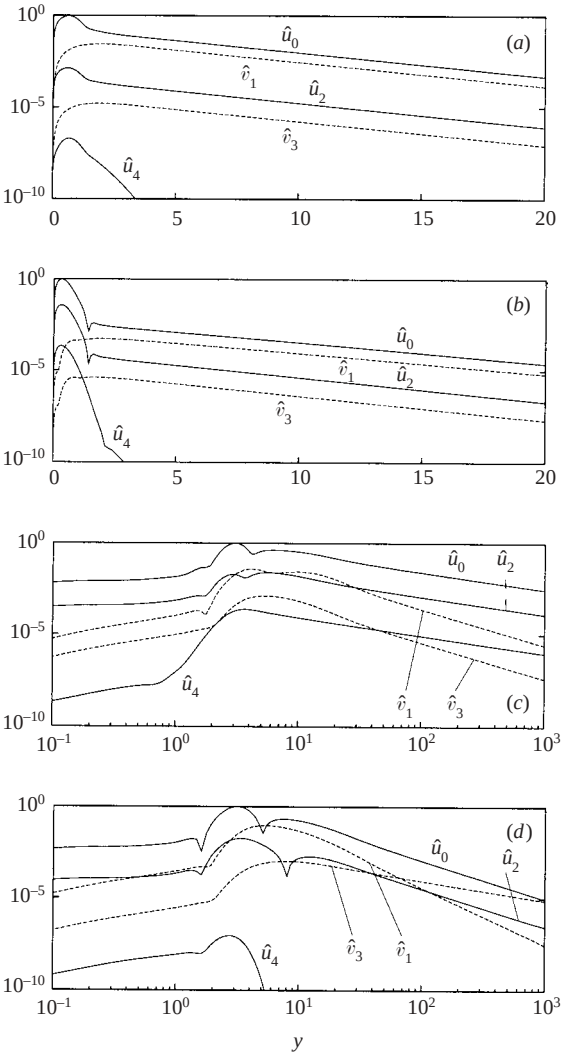

FIGURE 15. Eigenfunctions for $N=4$, $\beta=0.3$, $Re=1000$: (*a*) Tollmien–Schlichting mode, (*b*) least stable mode of the uniform branch, (*c*) algebraically decaying mode of type (4.4*c*), (*d*) algebraically decaying mode of type (4.4*a*); note the logarithmic scale of the abscissa in (*c*) and (*d*).

of the flow. For discrete modes with N odd, $\hat{v}$ dominates; the opposite is true for N even.

(*c*) As x becomes large the coefficient of the highest power in x determines the direction of the flow. The polynomial for $\hat{u}$ will be one order higher than the polynomial for $\hat{v}$. Thus, $\hat{u}$ will dominate within the boundary layer ($x \gg 1$, $y = O(1)$).

(*d*) For large x and large y, we have to consider the rate of decay of the highest-order solutions. Since $\hat{u}_N$ decays super-exponentially in y for all discrete modes the contribution of x^N vanishes compared to the other terms of lower order in x that decay only exponentially. Therefore, outside the boundary layer $\hat{u}$ is governed by a polynomial of order $N-2$ rather than N. The highest term of $\hat{v}$ is of order $N-1$, so the predominant direction of the flow in this region ($x \gg 1$, $y \gg 1$) is wall-normal for both symmetries.

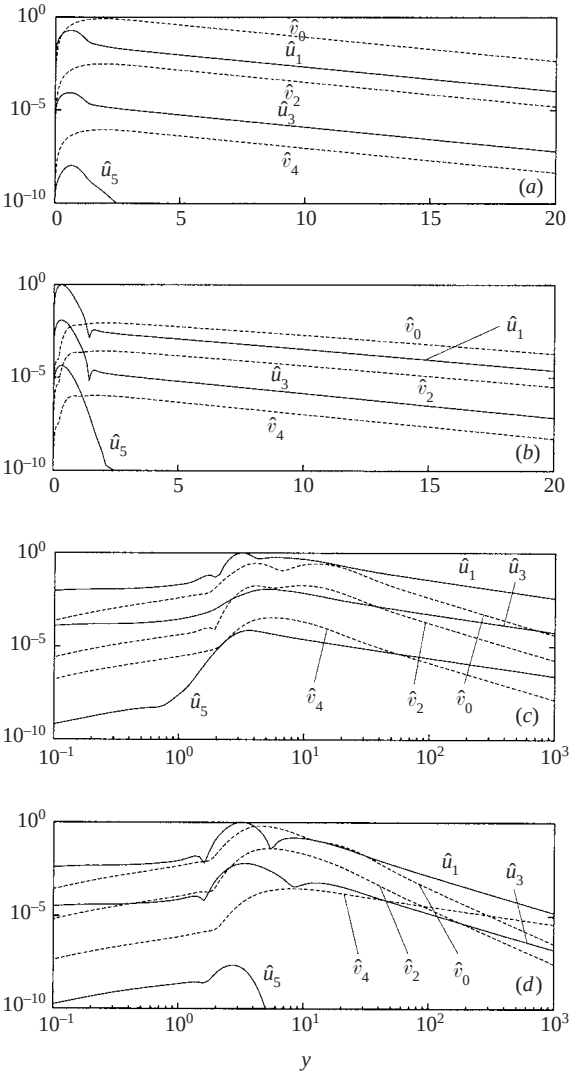

FIGURE 16. As figure 15 but for $N = 5$.

	$x = O(1)$		$x \gg 1$	
	Boundary layer	Free stream	Boundary layer	Free stream
N even	$\hat{u} \gg \hat{v}$	$\hat{u} \gg \hat{v}$	$\hat{u} \gg \hat{v}$	$\hat{v} \gg \hat{u}$
	$\hat{u} \gg \hat{v}$ (uniform branch)			
N odd	$\hat{v} \gg \hat{u}$ (upper and lower branches)	$\hat{v} \gg \hat{u}$	$\hat{u} \gg \hat{v}$	$\hat{v} \gg \hat{u}$

TABLE 1. Dominant velocity component in the discrete modes for different orders N and different locations in the flow field.

These results are summarized in table 1. In general we can state that the even modes are predominantly chordwise disturbances of the basic flow, whereas the odd modes disturb the flow mostly in the wall-normal direction.

5. Validity of the linear approximation

We must not forget that we have to take great care when linearizing the Navier–Stokes equations, particularly for higher-order modes ($N > 1$), as the validity of the linear approximation is compromised by two different effects. We will derive two relations that constrain (a) the amplitude of the disturbance and (b) the chordwise domain of validity for linear modes.

Before we derive these two constraints we have to quantify an observation made in the previous section. We saw that within a single mode the forced lower-order solutions have an increasingly higher amplitude (see, for example, figures 15 and 16). The reason for this becomes clear if we note that the right-hand side of the lower-order equations, i.e. the forcing term, consists of chordwise derivatives of the higher-order solutions. We can relate the coefficients of different orders as follows:

$$\frac{\hat{u}_m}{\hat{u}_n} = O\left(\frac{n!}{m!}\right), \tag{5.1}$$

with the same relation for the wall-normal velocity components $\hat{v}_n$. For clarity we will develop our arguments for the chordwise velocities $\hat{u}_n$ only.

In § 2 we perturbed the laminar flow by small velocities (u', v', w') which we take of $O(\epsilon)$. From (5.1) it follows that

$$\hat{u}_0 = O(\epsilon), \qquad \hat{u}_n = O\left(\frac{\epsilon}{n!}\right).$$

In the balance of order n we have a typical linear term of the form $Re^{-1}U\hat{u}_n$ that we will compare to nonlinear terms of the same order in x of the general form $v_{n-k}\partial_y u_k$ $(k = 0, \ldots, N)$. We require the nonlinear terms to be small compared to the linear terms. With the help of the relations above this requirement translates to

$$\frac{\epsilon}{Re\, n!} \gg \frac{\epsilon^2}{(n-k)!k!}.$$

This relation must be satisfied for all k and n ranging from 0 to N. The necessary and sufficient condition for this is

$$\epsilon \ll \frac{(N/2)!^2}{Re\, N!}. \tag{5.2}$$

By satisfying this constraint we ensure that equations up to order N can be linearized. However, this is not sufficient since there are also nonlinear terms of orders $N+1, \ldots, 2N-1$. To ensure that they remain small we have to bound the spatial domain of validity in the chordwise direction. We derive an explicit constraint by comparing linear terms of the form $Re^{-1}U\hat{u}_k$ to the nonlinear terms $\hat{v}_m\partial_y\hat{u}_n$. We then obtain the relation

$$\epsilon\frac{x^k}{Re\, k!} \gg \epsilon^2\frac{x^{m+n}}{m!\, n!},$$

with $k = 0, \ldots, N$, $n = 1, \ldots, N$, and $m = N+1-n, \ldots, N$. We obtain a necessary and sufficient condition for $k = N$, $n = N/2$, and $m = N/2$, in the form

$$x \ll \frac{(N/2)!^2}{\epsilon\, Re\, N!}. \tag{5.3}$$

The constraint (5.2) ensures that the right-hand side of (5.3) is large.

With the two constraints (5.2) and (5.3) the validity of the linear modes is clearly defined. Appropriate values of $\epsilon\, Re$ lie below the curve shown in figure 17. The curve decays rapidly, and physically relevant amplitudes ϵ can only be justified for small N.

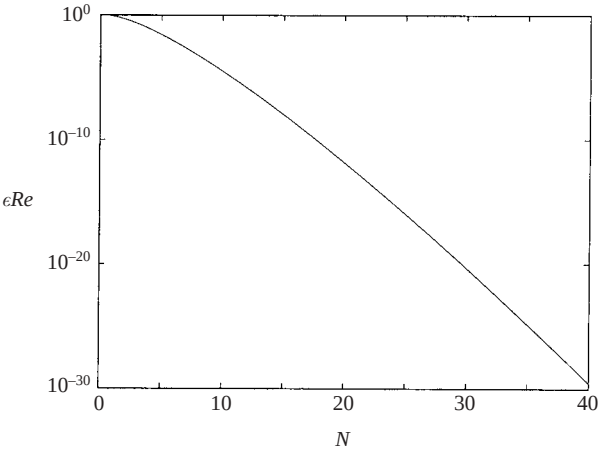

FIGURE 17. Bounding values of the constraint (5.2) for different values of N; valid choices for the disturbance amplitude ϵ have to lie sufficiently far beneath the curve shown.

The chordwise domain of validity is determined by the distance between the chosen ϵ and the curve. This distance corresponds to the logarithm of the right-hand side of (5.3). Thus, the farther the distance the larger the chordwise domain of validity.

To complete the discussion we should mention two important cases with different constraints. First, the uniform modes are solutions to the full Navier–Stokes equations. Thus, they are valid for any amplitude and over the entire spatial domain. Second, in the classical Görtler–Hämmerlin problem ($N = 1$) there is no constraint on the chordwise domain, since there are no nonlinear terms of order greater than 1. The only constraint is on the amplitude with $\epsilon \ll Re^{-1}$.

6. Summary and conclusions

We have studied the temporal stability problem of swept attachment-line boundary layers modelled by the swept Hiemenz equations. Starting with the global stability problem, a Hermite expansion has been identified by an asymptotic analysis as an advantageous transformation to convert the global stability problem into local (but coupled) stability problems. This coupling of the local stability problems has consequences for the eigenfunctions of higher-order modes and limits the validity of the linearization process that generated the governing equations in the first place. Estimates of the region of validity for both the amplitude and the chordwise extent have been presented.

The spectrum of the local stability problems showed a high degree of complexity which posed challenges to the numerical method as well as to the physical interpretation.

Nevertheless, the governing equations and the spectrum also revealed a substantial amount of structure that aided in the classification of modes by their symmetry (even versus odd), their order N (uniform, Görtler–Hämmerlin, higher-order) and their asymptotic behaviour (algebraic, exponential or super-exponential decay in the free stream). Table 2 summarizes these results.

For $N = 0$ we derived the uniform problem which serves as a prototype for the higher-order modes. It contains many of the main features of the global problem and its simple form makes it attractive for analytic studies. Algebraically and

Order	Eigenvalues	Eigenfunctions
$N=0$ (uniform modes)	continuous spectrum	algebraic decay $\sim y^{-\nu-1}$; standing waves in y travelling with the free-stream sweep flow
	continuous line spectrum at $c_r=1, c_i<0$	super-exponential decay $\sim y^{\nu}\exp(-y^2/2)$; maximum at edge of sweep flow boundary layer; standing waves in y travelling with the free-stream sweep flow; internal layer $\sim\exp[\pm(\beta Re(1-c))^{1/2}-y^2/4]$
	discrete modes; $c\propto(\beta Re)^{-1/3}$	super-exponential decay $\sim y^{\nu}\exp(-y^2/2)$; maximum inside boundary layer; internal layer $\sim\exp[\pm(\beta Re(1-c))^{1/2}-y^2/4]$
$N=1$ (Görtler–Hämmerlin modes)	2 continuous spectra, bounded by $c_i<-(\beta^2+2)/(\beta Re)$ for type (4.4a), and $c_i<-(\beta^2-1)/(\beta Re)$ for type (4.4c)	decay like (4.4a, c); type (4.4c) reaches into unstable half-plane
	continuous line spectrum at $c_r=1, c_i<0$	decay like (4.4f); $\hat{u}_0$ dominates
	continuous spectrum	decay like (4.4f); $\hat{v}_0$ dominates
	discrete spectrum: upper branch	Tollmien–Schlichting mode; decay like (4.4f); $\hat{v}_0$ dominates
	discrete spectrum: uniform branch; $c\propto(\beta Re)^{-1/3}$	decay like (4.4f); $\hat{u}_1$ dominates
	discrete spectrum: lower branch; $c\propto(\beta Re)^{-1/3}$	decay like (4.4f); $\hat{v}_0$ dominates
N even	same structure as Görtler–Hämmerlin spectrum, but shifted to lower c_i; algebraic spectra bounded by $c_i<-(\beta^2+N+1)/(\beta Re)$, and $c_i<-(\beta^2+N-2)/(\beta Re)$	highest order shows same characteristics as Görtler–Hämmerlin modes; lower order forced solutions have a larger amplitude, both velocity components decay like $\exp(-\beta y)$ or algebraically; $\hat{u}_0$ dominates close to the attachment-line
N odd	same structure as Görtler–Hämmerlin spectrum, but shifted to lower c_i; algebraic spectra bounded by $c_i<-(\beta^2+N+1)/(\beta Re)$, and $c_i<-(\beta^2+N-2)/(\beta Re)$	highest order shows same characteristics as Görtler–Hämmerlin modes; lower order forced solutions have a larger amplitude, both velocity components decay like $\exp(-\beta y)$ or algebraically

TABLE 2. Classification of the eigensolutions.

super-exponentially decaying modes were found where the super-exponentially decaying modes resemble a discrete Orr–Sommerfeld spectrum for a typical wall-bounded shear flow.

For $N=1$, the Görtler–Hämmerlin problem is recovered. Its most important feature is the existence of a Tollmien–Schlichting mode. In addition, it contains two new types

of mode: a second type of algebraically decaying mode and modes with exponential decay.

Higher-order modes ($N > 1$) reflect many features of the uniform and the Görtler–Hämmerlin modes; it was shown that even higher-order modes have a predominantly chordwise character, whereas odd modes have mostly a wall-normal character.

Algebraically decaying modes constitute the continuous spectrum which is needed for a complete description of the stability problem (similar to Blasius boundary layer flow; see Grosch & Salwen 1978). The exact location of the continuous spectrum remains an open question, but upper bounds for the growth rates are given in this study. We have to assume for now that the continuous spectrum covers large areas of the complex half-plane below this upper bound, but more work needs to be directed towards the exact location and role of the continuous spectrum.

In the light of the rich and complex structure of the spectrum it is instructive and desirable to use the initial-value problem governing the evolution of infinitesimal perturbations in the swept attachment-line boundary layer. This analysis is expected to shed further light on the interplay of discrete and continuous modes, on the role of various parts of the spectrum, and on the link between free-stream and boundary layer solutions. The companion paper (Obrist & Schmid 2003) will address certain issues related to the initial-value approach; a more comprehensive investigation is left for a future effort.

In connection with linear stability theory one often distinguishes the temporal and spatial problem. In the temporal problem we are interested in the evolution of the initial condition in time (initial value problem) whereas in the spatial problem we study the evolution of an inflow boundary condition in space (signalling problem). Gaster (1962) showed how temporal and spatial eigenvalues in the vicinity of the neutral curve are related to each other.

The temporal treatment of the stability problem addresses the situation where atmospheric disturbances enter the leading-edge area directly or are otherwise (impulsively) created inside the leading-edge boundary layer. The (spanwise) spatial stability problem examines the evolution of disturbances that originated upstream along the leading edge or even at the wing–fuselage junction (as suggested by Gaster 1965).

The present study has been concerned with the temporal stability problem, assuming a real spanwise wavenumber β and a specified spatial evolution in the chordwise direction, and solved for the temporal growth rate and phase velocity. To address the spatial evolution of disturbances by stability theory, two types of spatial growth are conceivable.

Assuming the frequency ω to be real and allowing the spanwise wavenumber β to take complex values addresses the spatial evolution of disturbances in the spanwise z-direction. This path has been taken by Joslin (1995) and Theofilis (1995) using direct numerical simulations. The corresponding spatial stability problem (4.1) poses an eigenvalue problem for β where β also appears quadratically. To obtain a linear eigenvalue problem a companion matrix technique has to be applied (see Lundbladh *et al.* 1994). The study of the spanwise spatial stability problem is beyond the scope of this study and will be left as a future effort.

Alternatively, one can also study the spatial evolution of disturbances in the chordwise direction. The order N of the Hermite polynomial takes the meaning of a streamwise wavenumber since Hermite polynomials (rather than exponentials) yield separability of the chordwise dependence. It is natural then to allow complex values of the polynomial order N to describe the spatial evolution of perturbations within

the mathematical framework presented here. We generalize the series expansion (3.2) as follows:

$$\hat{u}(x, y) = \sum_{n=0}^{\infty} \tilde{u}_n(y)\, \mathrm{e}^{x^2/2} \mathrm{D}_{N-n}(x), \tag{6.1}$$

$$\hat{v}(x, y) = \sum_{n=0}^{\infty} \tilde{v}_n(y)\, \mathrm{e}^{x^2/2} \mathrm{D}_{N-n}(x), \tag{6.2}$$

where $\mathrm{D}_{N-n}(y)$ are parabolic cylinder functions to allow for complex values of N. If N is a positive integer we recover the truncated Hermite series (3.2), since $\overline{\mathrm{He}}_N(x) = \exp(x^2/2)\mathrm{D}_N(x)$.

Bertolotti (1999) explored the spatial stability problem in this direction and found a new class of modes that are not polynomials in x. Setting $c = 0$ he found modal solutions that decay like x^{-N} as $x \to \infty$. When c coincides with one of the temporal eigenvalues the polynomial modes discussed in the previous sections are readily recovered. In the light of these findings, we have to restrict our previous statement – that all eigenfunctions are chordwise polynomials – to the eigenfunctions of the temporal problem.

We believe we have presented a mathematically rigorous and complete description of the temporal spectrum for swept attachment-line boundary flow which will lay the foundation for the analysis of non-modal effects and receptivity (Obrist & Schmid 2003) and should prove helpful in studying transition and flow control in swept attachment-line boundary layers.

We would like to thank Cray Inc. for financial support through an industrial student fellowship. DO. would like to thank Professor R. Friedrich from TU München and Professors V. Theofilis and U. Dallmann from DLR Göttingen. A significant part of this work was accomplished during visits to the TU München and DLR Göttingen.

REFERENCES

Abramowitz, M. & Stegun, I. A. 1965 *Handbook of Mathematical Functions*. Dover.

Bertolotti, F. P. 1999 On the connection between cross-flow vortices and attachment-line instabilities. In *Proc. IUTAM Symp. on Laminar-Turbulent Transition, Sedona* (ed. H. F. Fasel & W. S. Saric).

Boyd, J. P. 1982 The optimization of convergence for Chebyshev polynomial methods in an unbounded domain. *J. Comput. Phys.* **45**, 43–79.

Boyd, J. P. 1987 Orthogonal rational functions on a semi-infinite interval. *J. Comput. Phys.* **70**, 63–88.

Brattkus, K. & Davis, S. H. 1991 The linear stability of plane stagnation-point flow against general disturbances. *Q. J. Mech. Appl. Maths* **44**, 135–146.

Criminale, W. O., Jackson, T. L. & Lasseigne, D. G. 1994 Evolution of disturbances in stagnation-point flow. *J. Fluid Mech.* **270**, 331–347.

Cumpsty, N. A. & Head, M. R. 1969 The calculation of the three-dimensional turbulent boundary layer. Part III. Comparison of attachment line calculations with experiment. *Aero. Q.* **20**, 99–113.

Dallmann, U. 1980 Zur Stabilität dreidimensionaler Scherströmungen. Kriterien für reibungsfreie Störungsanregung. *DLR-FB* 80-05. DLR Göttingen.

Dhanak, M. R. & Stuart, J. T. 1995 Distortion of the stagnation-point flow due to cross-stream vorticity in the external flow. *Phil. Trans. R. Soc. Lond.* A **352**, 443–452.

Drazin, P. G. & Reid, W. H. 1981 *Hydrodynamic Stability*. Cambridge University Press.

Gaster, M. 1962 A note on the relation between temporally increasing and spatially increasing disturbances in hydrodynamic stability. *J. Fluid Mech.* **14**, 222–224.

Gaster, M. 1965 A simple device for preventing turbulent contamination on swept leading edges. *J. R. Aero. Soc.* **69**, 788–789.

Gaster, M. 1967 On the flow along swept leading edges. *Aero. Q.* **18**, 165–184.

Görtler, H. 1941 Instabilität laminarer Grenzschichten an konkaven Wänden gegenüber gewissen dreidimensionalen Störungen. *Z. Angew. Math. Mech.* **21**, 250.

Görtler, H. 1955 Dreidimensionale Instabilität der ebenen Staupunktsströmung gegenüber wirbelartigen Störungen. In *50 Jahre Grenzschichtforschung* (ed. H. Görtler & W. Tollmien). Vieweg, Braunschweig.

Gray, W. E. 1952*a* The effect of wing sweep on laminar flow. *Royal Aircraft Establishment, RAE TM* 255 (*ARC* 14, 929).

Gray, W. E. 1952*b* The nature of the boundary layer flow at the nose of a swept wing. *Royal Aircraft Establishment, RAE TM* 256 (*ARC* 15, 021).

Gregory, M. A. 1960 Transition and the spread of turbulence on a 60° swept-back wing. *J. R. Aero. Soc.* **64**, 562.

Grosch, C. E. & Salwen, H. 1978 The continuous spectrum of the Orr-Sommerfeld equation. Part 1. The spectrum and the eigenfunctions. *J. Fluid Mech.* **87**, 33–54.

Gustavsson, L. H. 1979 Initial-value problem for boundary layer flows. *Phys. Fluids* **22**, 1602–1605.

Hall, P. & Malik, M. R. 1986 On the instability of a three-dimensional attachment-line boundary layer: Weakly nonlinear theory and a numerical approach. *J. Fluid Mech.* **163**, 257–282.

Hall, P., Malik, M. R. & Poll, D. I. A. 1984 On the stability of an infinite swept attachment line boundary layer. *Proc. R. Soc. Lond.* A **395**, 229–245.

Hall, P. & Seddougui, S. O. 1990 Wave interactions in a three-dimensional attachment-line boundary layer. *J. Fluid Mech.* **217**, 367–390.

Hämmerlin, G. 1955 Zur Instabilitätstheorie der ebenen Staupunktsströmung. In *50 Jahre Grenzschichtforschung* (ed. H. Görtler & W. Tollmien). Vieweg, Braunschweig.

Hiemenz, K. 1911 Die Grenzschicht an einem in den gleichförmigen Flüssigkeitsstrom eingetauchten geraden Kreiszylinder. PhD thesis, Göttingen.

Jiménez, J., Martel, C., Agüi, J. C. & Zufiria, J. A. 1990 Direct numerical simulation of transition in the incompressible leading edge boundary layer. *ETSIA MF*-903. ETSIA Madrid.

Joslin, R. D. 1995 Direct simulation of evolution and control of three-dimensional instabilities in attachment-line boundary layers. *J. Fluid Mech.* **291**, 369–392.

Kestin, J. & Wood, R. T. 1970 On the stability of a two-dimensional stagnation flow. *J. Fluid Mech.* **44**, 461–479.

Lin, R.-S. & Malik, M. R. 1996 On the stability of attachment-line boundary layers. Part 1. The incompressible swept Hiemenz flow. *J. Fluid Mech.* **311**, 239–255.

Lundbladh, A., Schmid, P. J., Berlin, S. & Henningson, D. S. 1994 Simulation of bypass transition in spatially evolving flows. In *Proc. AGARD Symp. on Application of Direct and Large-Eddy Simulation to Transition and Turbulence*. AGARD CP-551.

Lyell, M. J. & Huerre, P. 1985 Linear and nonlinear stability of plane stagnation flow. *J. Fluid Mech.* **161**, 295–312.

Marcuse, D. 1991 *Theory of Dielectric Optical Waveguides*. Academic.

Obrist, D. & Schmid, P. J. 2003 On the linear stability of swept attachment-line boundary layer flow. Part 2. Non-modal effects and receptivity. *J. Fluid Mech.* **493**, 31–58.

Pfenninger, W. 1965 Flow phenomena at the leading edge of swept wings. In *Recent Developments in Boundary Layer Research – Part IV*. AGARDograph 97.

Pfenninger, W. 1977 Laminar Flow Control – Laminarization. Special Course on Concepts for Drag Reduction. *AGARD* 654.

Pfenninger, W. & Bacon, J. W. 1969 Amplified laminar boundary layer oscillations and transition at the front attachment line of a 45° swept flat-nosed wing with and without suction. In *Viscous Drag Reduction* (ed. C. S. Wells). Plenum.

Poll, D. I. A. 1979 Transition in the infinite swept attachment line boundary layer. *Aero. Q.* **30**, 607–629.

Rosenhead, L. 1963 *Laminar Boundary Layers*. Oxford University Press.

SPALART, P. R. 1988 Direct numerical study of leading-edge contamination. In *Proc. AGARD Symp. on Application of Direct and Large-Eddy Simulation to Transition and Turbulence*. AGARD CP-438.

THEOFILIS, V. 1995 Spatial stability of incompressible attachment-line flow. *Theor. Comput. Fluid Dyn.* **7**, 159–171.

THEOFILIS, V. 1998 On linear and nonlinear instability of the incompressible swept attachment-line boundary layer. *J. Fluid Mech.* **355**, 193–227.

TÜRKYILMAZOĞLU, M. & GAJJAR, J. S. B. 1999 On the absolute instability of the attachment-line and swept Hiemenz boundary layers. *Theor. Comput. Fluid Dyn.* **13**, 57–75.

WILSON, S. D. R. & GLADWELL, I. 1978 The stability of a two-dimensional stagnation flow to three-dimensional disturbances. *J. Fluid Mech.* **84**, 517–527.